Sana'a University Journal of Applied Sciences and Technology

Vol. 1 | No. 1 | Page 50 – 67 | 2023| https://jpurnals.su.edu.ye/jast

Electrochemical and Catalytic Properties of Au Nanoparticles

Yasmin M.S. Jamil[1,*], Mohammed Ahmed Hussein Awad[1,2], Hussein M.A. Al-Maydama[1]
[1] Department of Chemistry, Faculty of Science, Sana'a University, Yemen.
[2] Department of Chemistry, Faculty of Applied Sciences, Thamar University, Thamar, Yemen.
*E-mail: y.jamil@su.edu.ye; yasminjml@yahoo.com

ARTICLE INFO
Article history:
Received: January 13, 2023
Accepted: January 21, 2023
Published: January, 2023

Keywords
1. TiO_2 nanoparticles
2. Anodization
3. Photo deposition
4. Gold nanoparticles
5. Cyclic voltammetry

ABSTRACT: TiO_2 NPs powder (titanium oxide nanoparticles powder) is synthesized via anodization in 0.7 M $HClO_4$ is annealed in N_2 at 450°C for 3 hrs to obtain the TiO_2 NPs -N_2 powder as catalyst support to which Au is loaded via photodeposition technique using tetrachloroauric acid ($HAuCl_4$) and isopropanol as a sacrificial donor. The physicochemical characterizations of TiO_2 NPs arrays powder were performed by transmission electron microscopy (TEM). The TEM image suggested that Au nanoparticles were circular and there was a tendency of agglomerations. The electro-catalytic activity of Au NPs/TiO_2-NTs-N_2 catalysts in ferrocyanide system, KOH ,and H_2SO_4 electro-oxidation was examined by cyclic voltammetry (CV) and contrasted with a financially accessible polycrystalline gold electrode. Au-TiO_2 NPs-N_2 powder electrode catalyst displays a strikingly high electrocatalytic activity in KOH and H_2SO_4 solutions. The results contribute to Au NPs/TiO_2-NTs-N_2 catalysts as a potentially useful support material to enhance the good electro-catalytic efficiency for acidic and basic oxidation.

CONTENTS

1. INTRODUCTION

Noble metal nanoparticles and nanoclusters supported on metal oxides have gained much greater attention in recent years as a result of their numerous uses in heterogeneous catalysis [1]. Applications for metal nanoparticles supported on a semiconductor surface of a metal oxide include waste water treatment, purification,

medicine, photocatalytic synthesis of solar fuel, and industrial photocatalysis processes [2]. Nanoparticles can considerably improve the functionality and stability of semiconductors in reactions that are triggered by the absorption of light energy, according to Wenderich & Mul (2016).Cocatalyst nanoparticles can serve as (i) charge-carriers upon photoexcitation, inhibiting electron/hole recombination; (ii) active sites for processes requiring charge transfer; and (iii) stimulated light absorption, especially for gold and silver [2]. The use of nanomaterials to modify electrodes increases their surface area, which boosts the sensitivity of the electrochemical (bio)sensor. This is currently widely recognized.As a result, an electrode that has been changed with a nanomaterial has several potential uses, such as energy-conversion devices, chemical and biological sensors, and catalysis [3-6]. Carbon derivatives (carbon nanotubes (CNT), graphene oxide (GO), etc.) [7, 8], metallic nanoparticles (M NPs) (such as gold, silver, and copper) [9, 10], and their hybrids (M NPS/CNT, M NPs/GO, etc.) [11–13] are now the most commonly employed nanomaterials in this context. Due to their electrical, optical, catalytic, and magnetic capabilities, gold nanoparticles have generated a great deal of attention [14, 15]. Au NPs also increase transfer of electrons and boost analytical sensitivity [16]. The limitation of utilizing Au NPs is that their electrocatalytic properties depend on their size and shape. [17–19], necessitating control over the Au NPs' production process and immobilization technique on the electrode surface.

In the previous studies, the electrocatalyst Au NPs/ nano-diamond (ND)/carbon ionic liquid electrode (CILE) was characterized electrochemically by cyclic voltammetry in ferrocyanide system with peak anode current (I_{pa}) equals to (64.18 µA) , peak cathode current (I_{pc}) equals to (66.53 µA) and the ratio I_{pa}/ I_{pc} equals to 0.964 [20]. In our work the electrocatalyst Au NPs/TiO_2 NPs-N_2 was characterized electrochemically by cyclic voltammetry in ferrocyanide system with peak anode current (I_{pa}) equals to (2.751 mA/cm^2), peak cathode current (I_{pc}) equals to (-2.708 mA/cm^2) and the ratio I_{pa}/ I_{pc} equals to 1.02, that is to say with higher current.

Due to the relatively sluggish kinetics of oxygen formation and breakdown on the majority of electrodes, oxygen reduction reaction (ORR) considerably restricts the wide-ranging uses of fuel cells [21].In these applications, platinum and its alloys are primarily utilized as anode and cathode catalysts, but this metal is expensive and has a finite supply [22, 23].As a result, non-platinum electrocatalyst development has recently received significant scientific attention [24]. Gold has received less attention in electrocatalysis than the platinum-group metals, mostly due to its subpar catalytic activity. However, in ORR, bulk gold single-crystal electrodes with orientations (111), (110) and (100) show promising behavior. As a result, the ORR efficiency of an Au(100) electrode in an alkaline media is comparable to that of platinum [25]. Gold is often disseminated in the form of nanoparticles (NPs) and immobilized on a solid surface to achieve a high specific surface area and, in particular, to minimize the cost [26,27]. Semiconductive oxides are of great interest in the quest for support materials due to their excellent physical-chemical characteristics and high stability in acid and alkaline solutions [28]. In addition, as observed for the Pt/TiO_2 and Au/TiO_2 interfaces [29–32], noble metal NPs supported by semiconductive oxides may improve their catalytic activity due to a strong

metal support interaction (SMSI) impact. The effective oxygen electroreduction in an acidic solution on layers of ordered TiO_2 nanotubes loaded with Au NPs was recently reported by Macak et al. [33]. The functionalization of TiO_2 nanoparticle surfaces with metals including Au [34], Cu [35], Co [36], and Ag [37] has been documented in a number of papers. Noble metal nanoparticles at the TiO_2 surface that are exposed to radiation can take up electrons and stop the recombination of photo-generated electron-hole pairs [38, 39]. The Au nanoparticles deposited on titanium oxide nanoparticles annealed in nitrogen (Au NPs/TiO_2 NPs-N_2) powders were fabricated by photodeposition method using 400 W UV. The radiation with Ultraviolet (UV) was suitable for Au to be reduced and deposited onto the surface of titanium oxide nanoparticles annealed in nitrogen (i.e. TiO_2 NPs-N_2 powder) and hence, offered a sustainable synthesis method. This was attained during expositing catalyst support to 400 W UV, through which free electrons holes are produced. The electrons are excited into the conduction band (CB) which functions as an electron source for the gold cations reduction. The photoelectrons produced by the dint of titanium oxide nanoparticles reduce the Au^{+3} cation to Au metal nanoparticles. In the meantime, the photogenerated holes from the valance band (VB) react with isopropanol to form aldehyde [40-44]. The whole mechanism was shown in Fig. 1. The synthesized TiO_2 NPs displayed absolutely the anatase phase. On the other hand, the UV leads to the reduction and fixing of gold nanoparticles onto the surface of TiO_2 NPs-N_2 powder.

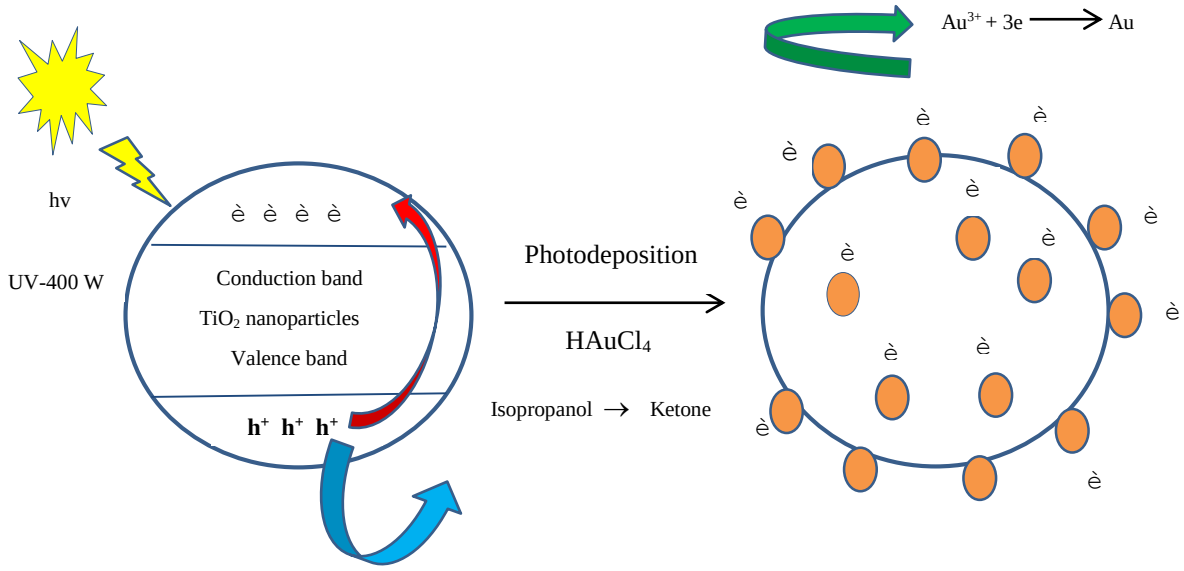

Figure (1): Mechanism of gold photodeposition (schematic representation for the preparation of Au NPs/TiO_2 NPs–N_2 catalyst using UV–400 W lamp photodeposition)

Catalysts made of gold nanoparticles are used in numerous chemical reactions. The surface of gold nanoparticles can be used for selective oxidation or, in some cases, can reduce a process. The production of gold nanoparticles for use in fuel cell applications has begun. These developments would help the auto and display sectors [45]. Au NPs are used for a

variety of purposes, including medication delivery [46], antibacterial [47], anti-cancer [48], antioxidant and catalytic activities [49], anticancer and anti-inflammatory activity [50], and drug delivery.

In order to compare the results with those of industrial polycrystalline gold, this work aims to examine the morphology and structure of Au NPs supported on TiO_2 nanoparticles as well as the electrocatalytic performances of gold nanoparticles in ferocyanide systems and in acidic and alkaline solutions. TiO_2 nanoparticles were coated with gold nanoparticles for this purpose.

2. EXPERIMENTAL

2.1. Materials:

Alfa Aesar Ti foils (>99.5% purity, 0.25 mm thick), perchloric acid $HClO_4$ (Perchloric acid 70 % $HClO_4$ (From MERCK) Made in Germany), the precursor tetrachloroauric acid ($HAuCl_4$, Sigma-Aldrich, 99.9%+%), isopropanol (99.0 %) as sacrificial donor From WINLAB, TiO_2 nanoparticles powder prepared in our lab with surface area 109m^2/g, Nafion (5 wt %), H_2SO_4 from Sigma–Aldrich, Flakes Extra Pure KOH From LOBA Chemie, India, potassium chloride GRG KCl (WINLAB), Potassium hexacyanoferrate (II) $K_4[Fe(CN)_6]$ Potassium hexacyanoferrate(III) trihydrate $K_3[Fe(CN)_6].3H_2O$ from MERCK.

2.2. Synthesis of TiO_2 nanoparticles powder

Titanium oxide nanoparticles powder (TiO_2 NPs) was prepared using the anodization process. The titanium foils were anodized in an aqueous solution containing 0.7 M per chloric acid ($HClO_4$) and were of >99.5% purity from Alfa Aesar. utilizing a two-electrode polypropylene electrochemical cell that operates at room temperature and 20V for an hour with a cathode made of Pt foil and Ti foil as the anode. A centrifuge was used to remove the TiO_2 NPs powder from the solution, and it was then dried overnight at 80°C. The TiO_2 NPs powder was subsequently annealed at 450 °C under N_2 for 3hs with 5 °C min^{-1} heating and cooling rates to obtain the TiO_2 NPs-N_2 powder [51].

2.3. Au photodeposition supported on catalyst supports

150 mg of catalyst support TiO_2 NPs-N_2 was mixed with 0.3 M of isopropanol and 10 mM of $HAuCl_4$ in a glass beaker and then irritated using a UV lamp (400W) for 2hrs under magnetic stirring. The intensity or power used during experiments was measured by Thorlab instrument at 380 nm wavelength and the power of 39 mW. During the irradiation of the solution, in the case of Au photodeposition on TiO_2 NPs-N_2 a color change from yellow to white was clearly obvious, indicating the adsorption of gold on the surface of TiO_2 NPs -N_2 powder.

The Au NPS/TiO_2 NPs-N_2 powder from the photodeposition was separated by centrifuging the solution and then the powder collected cleaned with deionized water and overnight 80°C drying. TiO_2 NPs-N_2 powder with loaded Au was used to prepare ink by weighing 50 mg of Au NPs/TiO_2 NPs-N_2 powder and the addition of 1ml DI (deionized) water plus 10 µL of 0.5 wt. % Nafion as a binder and then homogenized by using an ultrasonic bath to prepare the ink for the electrochemical experiments [51].

The electrochemical experiments were conducted in a conventional three-electrode cell with a solution of ferocyanide , 2M KOH and 1 M H_2SO_4. The working electrode consists of a platinum polycrystalline electrode with an area of 0.07 cm^2, and the counter electrode was platinum foil.

The saturated calomel electrode (SCE), which was connected to the cell via a Luggin capillary, served as the reference electrode. Using a micropipette, the electro catalyst (Au NPs/TiO_2 NPs-N_2) was loaded onto the electrode surface.

2.4. Physicochemical Characterizations

2.4.1. Transmission Electron Microscopy (TEM)

In order to conduct the physicochemical characterizations, the following was done: The TEM pictures used in our most recent work, which was reported elsewhere [51], were taken using a JEOL JEM-2100F electron microscope running at 200 kV.

2.5. Electrochemical Investigations:

Using a computerized potentiostat /galvanostat (Autolab, FRA2, AUTOLAB, TYPE III), CV was carried out in a typical three-electrode single-compartment Pyrex glass cell. SCE and pure Pt-foil were used as the reference and auxiliary electrodes, respectively.

Every potential given in the text was based only on the SCE electrode. Both a saturated calomel reference electrode (SCE) and a Pt wire auxiliary electrode were utilized. Also 3mm Pt polycrystalline working electrode was used (with a geometric surface 0.07 cm^2).The software program used in cyclic voltammetry measurements was NOVA 1.9. A consistently dispersed suspension ink (i.e. homogenized ink) was obtained by ultrasonicate the mixture of 50 mg catalyst and 1 mL deionized water for 30 min. Consequently, 3µL of the suspension product was applied to the Pt polycrystalline working electrode's surface (3 mm diameter, 0.07 cm^2). 1µL of Nafion (5 weight percent) solution was applied to the catalyst surface and dried once more at 40 °C. As a result, the working electrode was made, and the specific metal loading at the Pt operating electrode surface was around 0.020 mg (20.0 g) in 3µL of Au NPs/TiO_2 NPs-N_2 [51]. Electrochemical tests were performed in a ferocyanide system , 2M KOH and 1 M H_2SO_4 solutions. The mass loading in 3 µL of Au NPs/TiO_2 NPs-N_2 crystalline powder contains 0.020 mg Au. Then, using cyclic voltammetry (CV) in a 2.0 M KOH solution saturated with oxygen for 5 min., the electrocatalytic activity of the TiO_2 and Au NPs/TiO_2 NPs-N_2 electrodes in ORR was tested.

2.6. Material characterization:

A device for inductively coupled plasma spectroscopy was used to determine the mass loading of the Au in the produced materials of interest (ICPS-7000 ver.2 Shimadzu, SEQUENTIAL PLASMA SPECTROMETER). Samples were dissolved in aqua regia (3HCl:1HNO_3) acid using a high-pressure microwave digestion system in a Teflon tube vessel (MARSX; CEM) at 450K and 170 psi to make that determination. The digestive process was carried out using the Microwave Accelerated Reaction System (MARS) [51].

3. RESULTS & DISCUSSION:

3.1. Size and Morphology

In our very recent work published elsewhere [51], a typical TEM image of TiO_2 NPs-N_2 and Au NPs/TiO_2 NPs-N_2 was contained. It is evidenced that most TiO_2 NPs-N_2 are round. The nanoparticle average size of TiO_2 annealed in nitrogen particle size from the TEM image is 12.01 ±2.39 nm. The TEM images approve the formation of Au NPs/TiO_2 NPs-N_2 powder catalyst without varying the original morphology of TiO_2 nanoparticles and also confirming the gold nanoparticles size. The images prove that most Au-NPs are round and uniformly dispersed on the TiO_2 nanoparticles annealed in N_2 support with agglomerations, confirming that most Au NPs/TiO_2 NPs-N_2 are also round. The average size of the Au Nanoparticles in the TEM image is 23.18± 4.39 nm. Equation (1) was used to determine the typical number of gold atoms in each nanoparticle. A spherical form was presumed in order to calculate the typical amount of gold atoms that are present in a nanoparticle.

This estimate was made using Equation (1).

$$N = \pi\rho\ N_A\ D^3/\ 6\ M \qquad (1)$$

Where M is the atomic mass of gold (197 g/mol), ρ is the density of gold (1.93 x 10^{-20} g/nm^3), NA is the Avogadro constant of element atoms (6.02214179 x 10^{23}), and D is the average diameter of nanoparticles in nm [52].

3.2. Electrochemical Investigations of Au NP/TiO_2 NPs-N_2 catalyst

3.2.1. Cyclic Voltammetry in Ferrocyanide System

Figure 2. shows the CV profile of 10mM K_4 [Fe (CN) $_6$] + K_3 [Fe (CN)$_6$] + 0.5 M KCl on Au NPs/TiO_2 NPs-N_2 , Au polycrystalline working electrode and Pt polycrystalline working electrode. For Au polycrystalline working electrode, Peak-to-peak separation (ΔE_p) for the 10 mM Potassium ferrocyanide/ ferric cyanide complex (10 mM $[Fe(CN)_6]^{3-/4-}$) was 70 mV at 50 mV/s, which is close to the theoretical value of 59/n mV, where n=1. The relationship between the backward and forward peak currents (I_{pa}/I_{pc}) was 0.98, meaning that the amount of redox mediator is almost the same. All the data proved that the characteristic electrochemical behavior of Au NPs in potassium ferricyanide solution Fe (III)/Fe (II) was realized with an approximately reversible process [53]. A definite decrease in the current and an increase in the (ΔE_p) were seen when Au NPs were added to the TiO_2 NPs-N_2 electrode. The nanoparticles' impact on the electronic transfer makes it more challenging and eliminates the couple's ability to reverse the process. It is clear from Table 1 that the ratio (I_{pa}/I_{pc}) remained constant, indicating that the same quantity of redox mediator is reduced and oxidized. Additionally, it is evident from this table that the (ΔE_p) declines in the following order: Au polycrystalline electrode < Au NPs/TiO_2 NPs-N_2 < Pt polycrystalline electrode. The order follows the same pattern as the active surface area, according to Table 1. Therefore, Au WE has the biggest active surface area and the most heterogeneous film. The smallest ΔE_p means high electrical conductivity.

As can be seen in Fig. **2**, the Au NPs/TiO_2 NPs-N_2 electrodes obtained by photo-deposition showing a typical Nernstian behavior. The values of the pertinent parameters E^0 = 249 mV, ΔE_p = 76 mV, and i_{ap}/i_{cp} = 1.02 (n = 1) clearly show that the

electrodes' response is repeatable and comparable to those of gold electrodes that have been constructed.

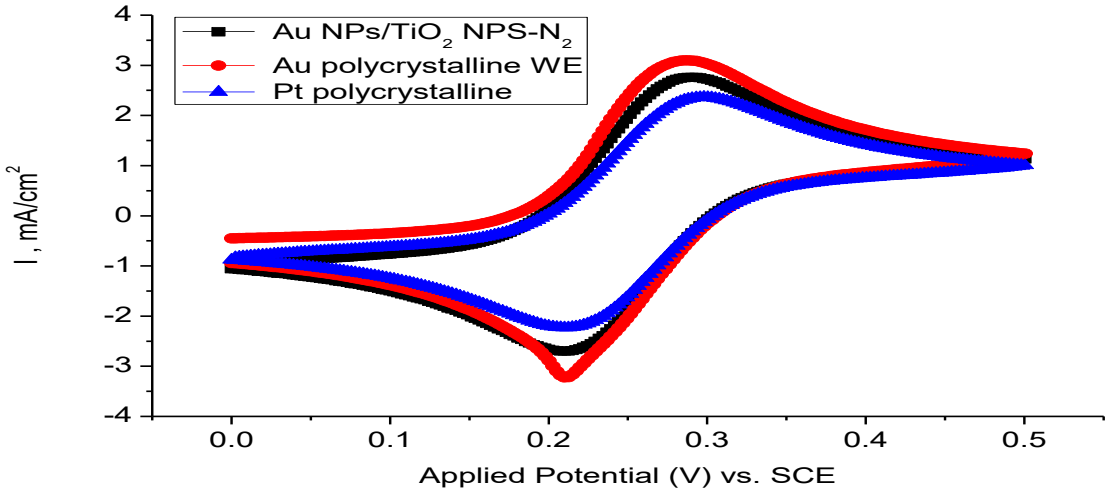

Figure (2): CVs of 10mM K_4 [Fe (CN) $_6$] + K_3 [Fe (CN)$_6$] + 0.5 M KCl, scan rate 50 mV/s, contains Au NPs/TiO_2 NPs-N_2 powder , in contrast with Au polycrystalline and Pt polycrystalline electrodes with area 0.07 cm^2 , window of potential range 0-0.5V.

Table 1 includes the values of I_{pa}/I_{pc} for the 0.07 cm^2 Au and Pt polycrystalline working electrodes as well as the I_{pa} (peak height-mA/cm^2) for the anodic and cathodic paths.

Table 1: Comparison between Au NPs/TiO_2 NPs-N_2 powder and 0.07 cm^2 Au and Pt polycrystalline working electrodes in ferrocyanide system.

Electrode	I_{pa} (mA/cm^2)	I_{pc} (mA/cm^2)	I_{pa}/ I_{pc}
Au NPs/TiO_2 NPs-N_2	2.751	- 2.708	1.02
Au polycrystalline electrode	3.172	- 3.233	0.981
Pt polycrystalline	2.408	- 2.209	1.09

Table 2: Oxidation and reduction peaks of potentials, reduction/oxidation peaks separation and also ΔG°(kJ) of Au NPs/TiO_2 NPs-N_2 and 0.07 cm^2 Au and Pt polycrystalline working electrodes in ferrocyanide system.

Electrode	E_{pa}(V)	E_{pc}(V)	ΔE (V)	ΔE(mV)	E°(V)	ΔG°(kJ)
Au NPs/TiO_2 NPs-N_2	0.287	0.211	0.076	76	0.249	-24.03
Au polycrystalline electrode with area 0.07 cm^2	0.284	0.211	0.073	73	0.248	-23.93
Pt polycrystalline electrode with area 0.07 cm^2	0.290	0.210	0.08	80	0.25	-24.12

Using $[Fe(CN)_6]^{3-/4-}$ redox probes, the electron transfer properties of the surfaces of various electrodes were investigated by CV, as shown in Figure 2. The Au NPs/TiO_2 NPs-N_2 electrode had higher $[Fe(CN)_6]^{3-/4-}$ redox currents than the bare Pt polycrystalline electrode. Due to TiO_2 NPs-N_2's excellent ability to transfer electrons, the potential difference between the $[Fe(CN)_6]^{3-/4-}$ redox probe's oxidation and reduction peaks also decreased. When compared to bare Pt polycrystalline electrodes, the redox currents of the redox probes were further increased on Au NPs/TiO_2 NPs-N_2, proving that the Au NPs significantly increased the electron transfer capabilities [54]. The Au NPs/TiO_2 NTs-N_2 samples were evaluated as electrodes using a one electron redox couple to make sure that there was good electrical contact between the gold and the titanium electrode beneath it. Voltammetric curves for the reduction of $K_3Fe(CN)_6$ are shown in Fig. 2 for Au NPs/TiO_2 NTs-N_2 electrodes, Au polycrystalline electrodes with an area of 0.07 cm^2, and Pt polycrystalline electrodes with an area of 0.07 cm^2. The expected reversible behavior for the reduction on Pt polycrystalline electrode is visible in the voltammogram for the Au NPs/TiO_2 NTs-N_2 electrodes. It implies that the titanium and the electrodeposited gold sheet have pretty acceptable adhesion and electrical contact. In order to compare the prepared electrodes with a pure gold electrode and to electrochemically characterize the real surface of the Au NPs/TiO_2 NTs-N_2 electrode, the surface area of the electrode was determined using 10 mM $K_4Fe(CN)_6$ in 0.5 M KCl by recording the cyclic voltamograms. From the cyclic voltammetric peak current and the diffusion coefficient of hexacyanoferrate, the surface area of the electrode was calculated by using the Randles-Sevcik equation (2) [55-57]:

$$i_{pa} = (2.69 \times 10^5)\, n^{3/2}\, A\, D_o^{1/2}\, \nu^{1/2}\, C_o \qquad (2)$$

$$A = i_{pa} / (2.69 \times 10^5)\, n^{3/2}\, D_o^{1/2}\, \nu^{1/2}\, C_o \qquad (3)$$

where i_{pa} is the peak current of anode in mA, the number of electrons transported, or n, is 1, the electrode's surface area is A, the diffusion coefficient, or D_o, is 9.382 10^{-6} cm^2 s^{-1}, the scan rate, or v, is 50 $mV \cdot s^{-1}$, and the concentration of electroactive species, or C_o, is expressed in moles/cm^3 (0.5 M KCl). The surface area (geometric area) of the three electrodes calculated using the Randles-Sevcik equation was approximately close to the surface area of the three electrodes that were found practically (0.07 cm^2).

3.2.2. Cyclic Voltammetry in 2 M KOH System

Cyclic voltammograms of commercial Au disk (Au working electrode) and Au NPs/TiO_2 NPs-N_2 electrodes in alkaline supporting electrolyte were conducted and shown in Figure 3. The voltammograms of an Au disk electrode and Au NPs/TiO_2 NPs-N_2 recorded in 2.0 M KOH under N_2 saturation displayed three regions according to the applied potential (Figure 3). The regions in Figure 3 are: (I) is the oxidation peak of Au catalyst; (II) is oxygen evolution, (III) is the reduction peak of Au catalyst and (IV) is oxygen reduction, The adsorption (oxidation peaks) and desorption (reduction peak) of oxygenated species at the electrode surface are visible in region (IV) at higher potentials. Small currents connected to the

charge and discharge of the double-layer capacity are characteristic of the double-layer region (V), where no net electrochemical reaction occurs [58,59]. The hydrogen region vanished in the Au electrode's case.

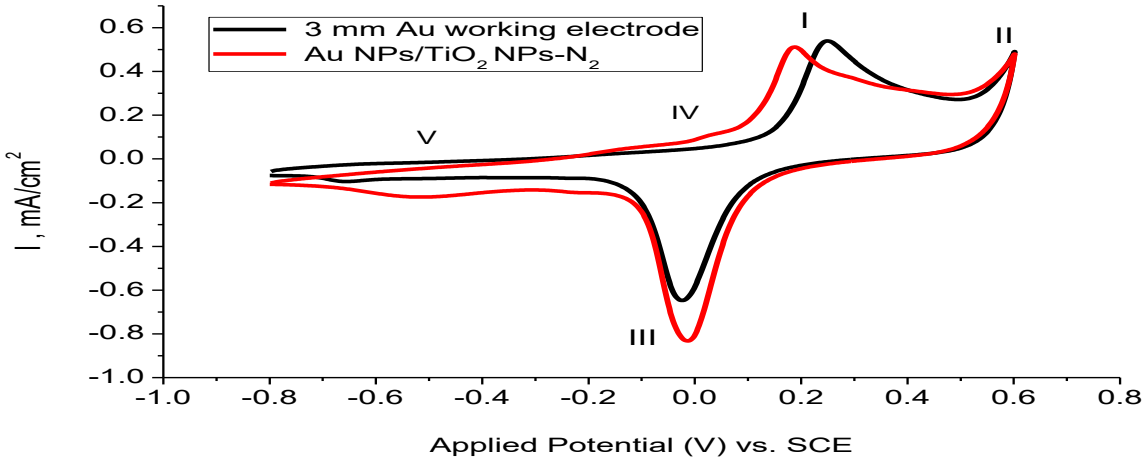

Figure (3): CV of 3 mm Au working electrode, Au NPs/TiO_2 NPs-N_2 powder all in 2 M KOH purged in saturated N_2 for 3 min at a scan rate of 50 mV/s.

Two oxidation and one reduction reactions are seen when the nanosized gold electrode is cycled in an alkaline solution (Figure 3). The creation of the oxide layer Au-O and the anodic peaks at 0.2 and 0.6 V are typically attributed to each other [60, 61] and are followed by reduction of Au-O at -0.02 V in the cathodic scan [61]. In both acidic and alkaline liquids, the polycrystalline commercial electrode exhibits qualitatively identical curves.

A CV scan was carried out in 2.0 M KOH from (-0.8-0.7 V) at 50 mVs^{-1} to determine the electrochemical active surface area (ECSA-ECSA) of the Au NPs-TiO_2 NPs-N_2 catalyst as it had been constructed. The final cycle is shown in Fig. 3. The creation and reduction of a monolayer of Au oxide are attributed to the anodic peak on the forward scan and the cathodic peak on the backward scan, respectively [69]. The ECSA of Au NPs-TiO_2 NPs-N_2 catalyst is 19.05cm^2 mg^{-1} and for Au polycrystalline working electrode is 15.90cm^2 mg^{-1}, which were calculated using a double layer correction and a charge density of 0.386 mC cm^{-2} [62] from the reduction peak at -0.0114V and -0.0237V, respectively.

The equations (4) and (5), which are mentioned in our most recent work that was published elsewhere [63], were used to determine the electrochemical active surface area (ECSA-ECSA) of the Au NPs-TiO_2 NPs-N_2 catalyst as it had been produced in 2 M KOH.

$$Q_h = \frac{\text{Peak area (mA.V)}}{\text{Scan rate } (\frac{V}{s})} \quad (4)$$

ECSA = Q_h in mC / q (constant in mC/cm^2) (5)

3.2.3. Cyclic Voltammetry in 1 M H_2SO_4 System

Overlap between the oxidation peaks of Au working electrode and the Au NPs-TiO_2 NPs-N_2 powder was observed , therefore Au

catalyst could not be loaded on Au working electrode. From Figure 4 , Peak (a) is the anodic oxidation peak of gold polycrystalline working electrode and Au NPs-TiO_2 NPs-N_2 powder crystalline, peak (b) is oxygen evolution, (c) is the cathodic reduction peak of gold surface oxide and Au NPs-TiO_2 NPs-N_2 powder crystalline, peak (d) is the desorption of chloride traces that result from $HAuCl_4$ and the peak (e) is the adsorption of chloride traces that result from $HAuCl_4$.

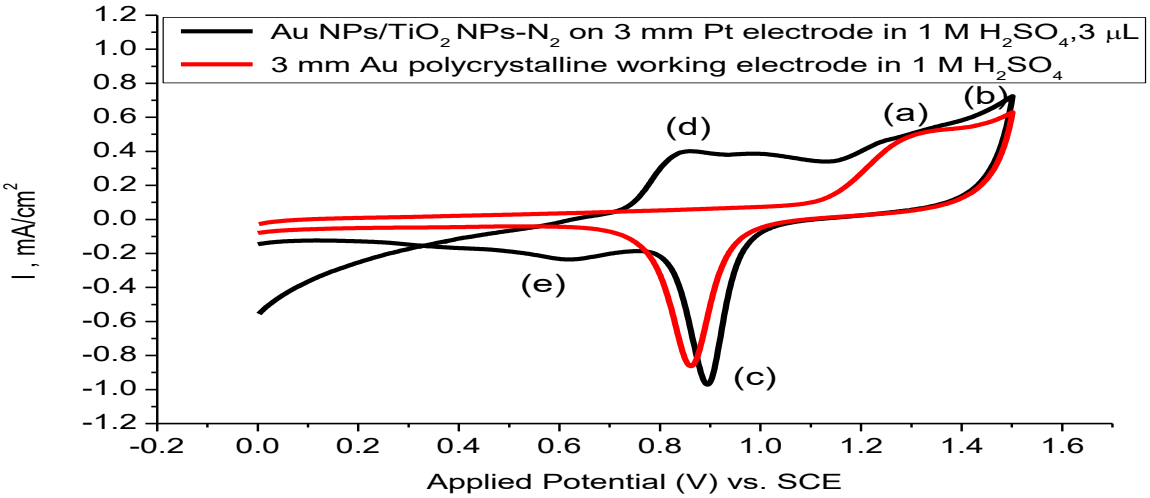

Figure (4) : CV of Au polycrystalline working electrode and photodeposition of 3 microliter Au NPs-TiO_2 NPs-N_2 powder crystalline was loaded on 3 mm Pt polycrystalline working electrode , all in 1 M H_2SO_4 at a scan rate of 50 mV/s.

Figure 5 shows the anodic peak (a) and cathodic peak (c), that are assigned to the oxidation of gold and reduction of gold surface oxide, respectively. Peak (b) is oxygen evolution while adsorption of protons occurs in the region (d) i.e. oxygen reduction and region to the left of d is hydrogen evolution.

Figure 5 shows a cyclic voltammogram of a 3 mm Au polycrystalline working electrode at potentials of 0 V to 1.5 V set at a scan rate of 50 mV/s. The oxidative peaks, a and b, are related to the evolution of oxygen and the oxidation of deposited gold to Au(III), respectively.

The reduction of gold surface oxide (at 0.88 V), the reduction of protons, and hydrogen evolution, respectively, are attributed to the reductive peaks c, d, and e [64–66]. The reduction peak in the second cycle, as shown in Figure 5, has moved to a higher positive potential, facilitating the electrodeposition of gold on the gold nuclei that have already been deposited [67]. Golden-colored deposits can be seen when the potential is cycled from 0.0 V to 1.5 V, especially at greater concentrations of the gold deposition solutions and during longer deposition durations. More gold is put onto the substrate over a longer period of time, although some electrodeposited particles are

not spherical, which may have led to aggregation formation.

Figure 5 illustrates how the activation/stabilization CV scans of Nano-sized electrode material on a Pt polycrystalline electrode demonstrate the well-known behavior of gold when used in a strongly acidic solution [68]. The creation of a thin oxide layer on the gold surface is what causes the oxidation process to occur at high potential (1.3 V); the layer is subsequently reduced during the cathodic sweep at potentials about 0.896 V.

After 15 cycles, no discernible variations between two subsequent scans were found.

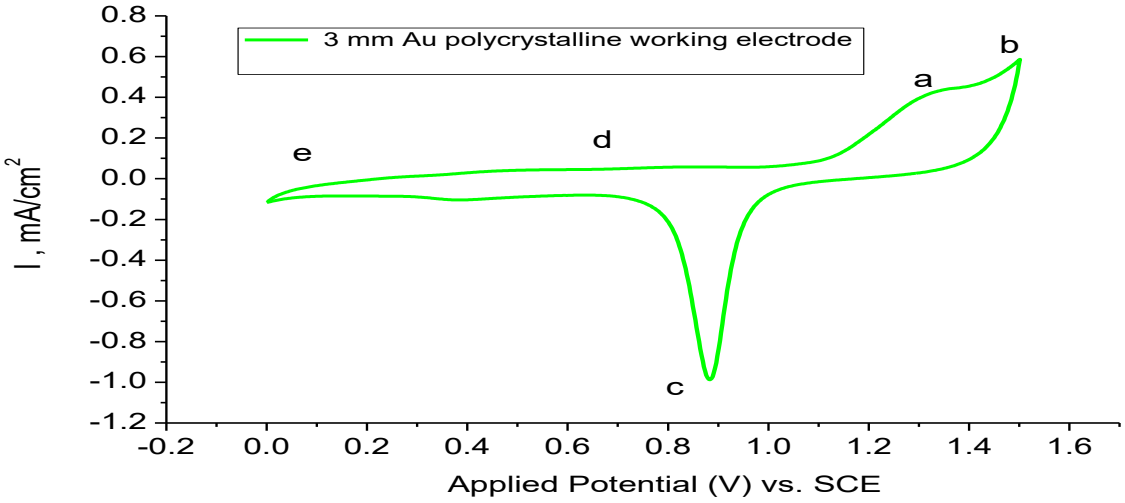

Figure (5): CV of 3 mm Au polycrystalline working electrode in 1 M H_2SO_4 at a scan rate of 50 mV/s.

A CV scan was carried out in 1.0 M H_2SO_4 from 0 -1.6 V at 50 mV s^{-1} to determine the electrochemical active surface area (ECSA-ECSA) of the Au NPs-TiO_2 NPs-N_2 catalyst as it had been constructed. The final cycle is shown in Fig. 4. The creation and reduction of a monolayer of Au oxide are attributed to the anodic peak on the forward scan and the cathodic peak on the backward scan. With a double layer correction and a charge density of 0.386 mC cm^{-2}, the ECSA of the Au NPs-TiO_2 NPs-N_2 catalyst was calculated to be 14.0 cm^2 mg^{-1}.

Based on the generated cyclic voltammograms, the total charge of the hydrogen desorption area (Q_H) with the correction of the double layer region as shown in Eq.6 could be used to calculate the real surface area (A_r) or electrochemical active surface area (EASA-ECSA) of the Au NPs-TiO_2 NPs-N_2 electrode. During the experiment, the theoretical charge of 0.386 mC/cm^2 (Q_m), which corresponds to the desorption of monolayer hydrogen on smooth Au [69], was taken into account.

$$Q_H = \frac{1}{V_b}\int_{E_1}^{E_2} I.dE \qquad (6)$$

where I is the current density ($mAcm^{-2}$) and Vb is the scan rate, and dE is the potential (mV) ($mV.s^{-1}$). Thus, the following formulas can be used to get the real surface area (A_r) and roughness factors (R_f) of the final electrode:

$$A_r \text{ (EASA-ECSA)} = Q_H/Q_m \qquad (7)$$

$$R_f = A_r \text{ (EASA-ECSA)}/A_g \qquad (8)$$

where A_g is the prepared electrode's geometric area, which is equal to 0.07 cm^2.

Normally, electrocatalyst performance is assessed using the electrochemical active surface area (EASA-ECSA). The roughness factor is directly proportional to electrochemical active surface area i.e. increasing of roughness factor indicating to increase of electrochemical active surface area. According to the reduction peak charge and ICP analysis, Table 3 shows the electrochemical active surface area, roughness factors (R_f), and mass loading of Au NPs catalysts. However, the Au NPs-TiO_2 NPs-N_2 shows lower roughness factor than that for Au polycrystalline working electrode as shown in Table 3.

Table 3: Electrochemical active surface area (ECSA) and roughness factors (R_f) of Au polycrystalline working electrode and Au NPs/TiO_2 NPs-N_2 powder in 1 M H_2SO_4.

Catalysts	Q_H (charge density), mC	Surface area (cm^2) (ECSA)	R_f	Mass loading (g/cm^2)
Au polycrystalline working electrode	0.113	0.29	4.1	----------
Au NPs/TiO_2 NPs-N_2 powder	0.108	0.28	4.0	2.86×10^{-4}

The Au polycrystalline electrode had an electrochemical active surface area (EASA-ECSA) of 0.29 cm^2, while the Au NPs/TiO_2 NTs-N_2 electrode had a lower EASA-ECSA of 0.28 cm^2.

Au NPs-TiO_2 NPs-N_2 powder electrode can be used as chloride sensors in acidic solution (1 M H_2SO_4). We note that desorption and adsorption of chloride take place on TiO_2 NPs-N_2 powder during photo deposition of $HAuCl_4$ and in cyclic voltammetry of Au NPs-TiO_2 NPs-N_2 in acidic medium (1 M H_2SO_4) the peaks of chloride appear, i.e. the desorption of chloride traces that result from $HAuCl_3$ (d) and adsorption of chloride traces that result from $HAuCl_4$ (e).To remove these peaks we must make treatment the powder of Au NPs-TiO_2 NPs-N_2 with 0.1 M KOH i.e. washing the powder of Au NPs-TiO_2 NPs-N_2 with 0.1 M KOH to remove chloride where OH^- replaces Cl^-.

$$KOH + Cl^- \rightarrow KCl + OH^- \qquad (9)$$

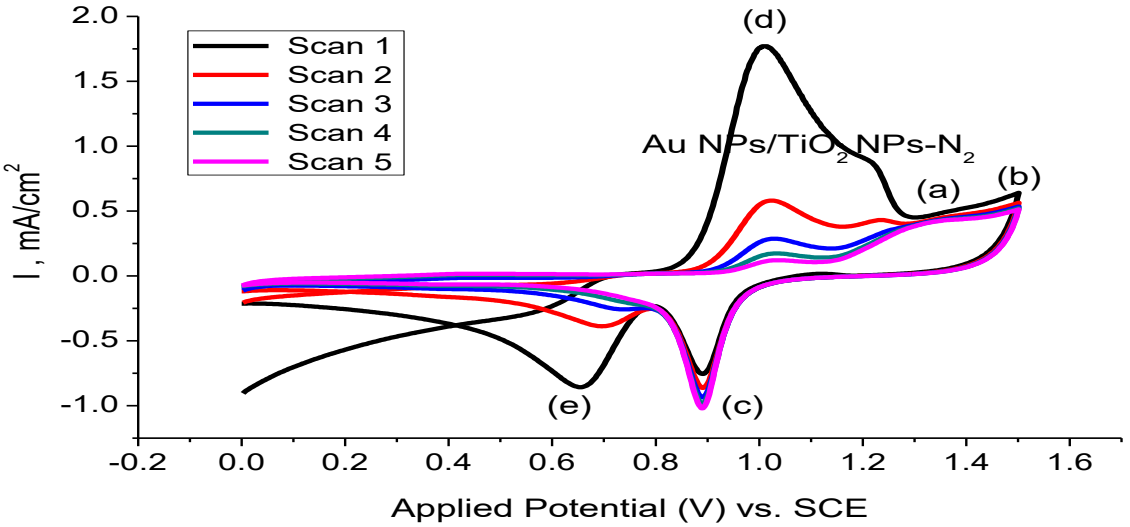

Figure (6): CV for photodeposition of Au NPs-TiO_2 NPs-N_2 powder on 3 mm Au working electrode in 1 M H_2SO_4 at a scan rate was 50 mV/s (effect of scan).

In 1 M $HClO_4$ at 50 mV/s with a potential domain between -500 and 1700 mV, the Au polycrystalline working electrode and Au NPs-TiO_2 NPs-N_2 powder electrodes were subjected to cyclic voltammetry tests. Voltammograms typically reveal a clean gold surface, as shown in Fig. 7.

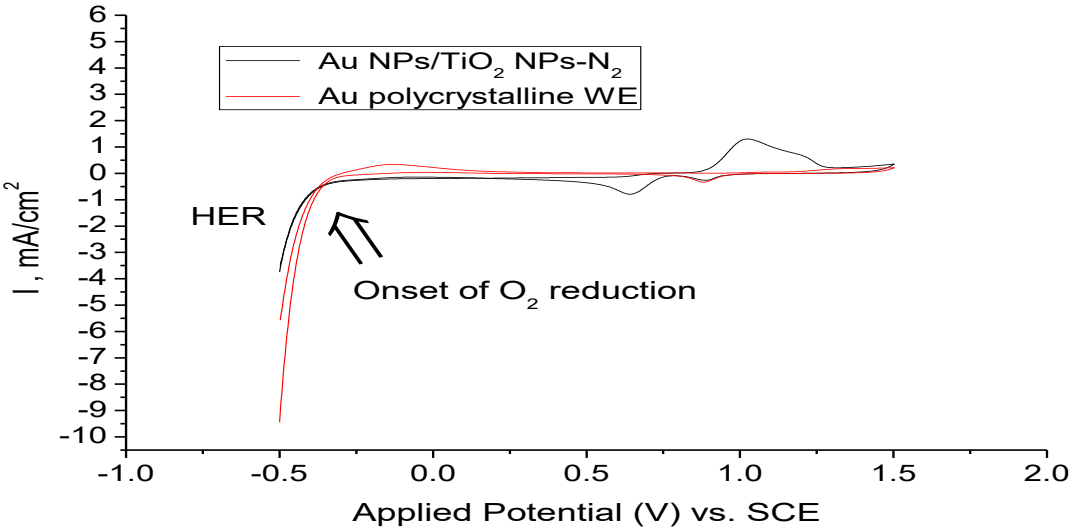

Figure (7): CV for Au polycrystalline working electrode and photodeposition of Au NPs/TiO_2 NPs-N_2 powder 10 μL loaded on 3 mm Pt working electrode all in 1 M $HClO_4$ at a scan rate was 50mV/s (potential range from -0.5 V to 1.5 V).

The cyclic voltammograms of 10µL saturated KCl on 3 mm Au electrode were performed in 1 M $HClO_4$ at 50 mV/s and a potential domain between 0 and 1500 mV as in Figure 8.

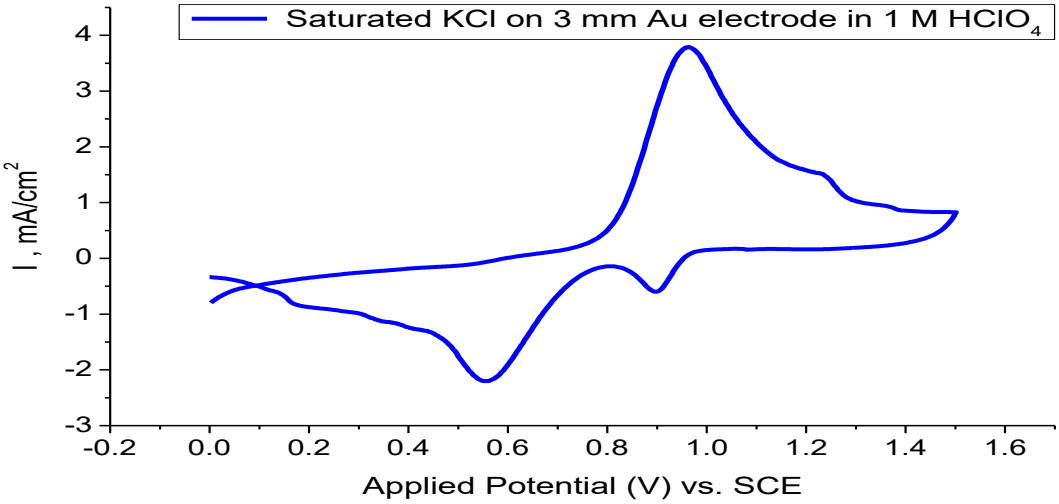

Figure (8): Saturated KCl on 3 mm Au electrode in 1 M $HClO_4$ at scan rate was 50 mVs^{-1}, 10µL.

4. CONCLUSIONS:

Using tetrachloroauric acid ($HAuCl_4$) and isopropanol as sacrificial donors, a gold nanoparticle electrode was created by photodepositing gold metal onto TiO_2 nanoparticles that had been annealed in a N_2 electrode. The circular shape of the particles could be seen in the TEM image of the Au NPs/TiO_2 NPs-N_2. In KOH and H_2SO_4 solutions, the gold nanoparticles outperform commercially available polycrystalline electrodes in terms of electrocatalytic characteristics. In the ferro cyanide system, the Au-NPs/TiO_2-NTs electrode displayed significantly greater currents than the Pt polycrystalline electrode. Chloride sensors in acidic solutions can be made from Au NPs-TiO_2 NPs-N_2 powder electrodes (1 M H_2SO_4).

5. REFERENCES:

[1] C. C. Chusuei, X. Lai, K. A. Davis, E. K. Bowers, J. P. Fackler, and D. W. Goodman, A Nanoscale Model Catalyst Preparation: Solution Deposition of Phosphine-Stabilized Gold Clusters onto a Planar TiO_2 (110) Support, Langmuir. 17 (2001) 4113-4117. https://doi.org/10.1021/la001684r.

[2] K. Wenderich, G. Mul, Methods, Mechanism, and Applications of Photodeposition in Photocatalysis: A Review, Chemical Reviews. 116 (2016) 14587-14619. https://doi.org/10.1021/acs.chemrev.6b00327.

[3] N. Jadon, R. Jain, S. Sharma, K. Singh, Recent trends in electrochemical sensors for multianalyte detection – A review, Talanta. 161 (2016) 894-916. https://doi.org/10.1016/j.talanta.2016.08.084.

[4] P. Sierra-Rosales, C. Toledo-Neira, J. Squella, Electrochemical determination of food colorants in soft drinks using MWCNT-modified GCEs, Sensors And Actuators B: Chemical. 240 (2017) 1257-1264. https://doi.org/10.1016/j.snb.2016.08.135.

[5] Y. Zhang, Q. Wei, The role of nanomaterials in electroanalytical biosensors: A mini review, Journal Of Electroanalytical Chemistry. 781 (2016) 401-409. https://doi.org/10.1016/j.jelechem.2016.09.011.

[6] P. Rasheed, N. Sandhyarani, Electrochemical DNA sensors based on the use of gold nanoparticles: a review on recent developments, Microchimica Acta. 184 (2017) 981-1000. https://doi.org/10.1007/s00604-017-2143-1.

[7] Ö. Yokuş, F. Kardaş, O. Akyıldırım, T. Eren, N. Atar, M. Yola, Sensitive voltammetric sensor based on polyoxometalate/reduced graphene oxide nanomaterial: Application to the simultaneous determination of l-tyrosine and l-tryptophan, Sensors And Actuators B: Chemical. 233 (2016) 47-54. https://doi.org/10.1016/j.snb.2016.04.050.

[8] M. Yola, N. Atar, A Highly Efficient Nanomaterial with Molecular Imprinting Polymer: Carbon Nitride Nanotubes Decorated with Graphene Quantum Dots for Sensitive Electrochemical Determination of Chlorpyrifos, Journal Of The Electrochemical Society. 164 (2017) B223-B229. https://doi.org/10.1149/2.1411706jes.

[9] S. Narwade, B. Mulik, S. Mali, B. Sathe, Silver nanoparticles sensitized C60(Ag@C60) as efficient electrocatalysts for hydrazine oxidation: Implication for hydrogen generation reaction, Applied Surface Science. 396 (2017) 939-944. https://doi.org/10.1016/j.apsusc.2016.11.065.

[10] M. Yola, N. Atar, T. Eren, H. Karimi-Maleh, S. Wang, Sensitive and selective determination of aqueous triclosan based on gold nanoparticles on polyoxometalate/reduced graphene oxide nanohybrid, RSC Advances. 5 (2015) 65953-65962. https://doi.org/10.1039/c5ra07443f.

[11] M. Yola, T. Eren, N. Atar, A novel and sensitive electrochemical DNA biosensor based on Fe@Au nanoparticles decorated graphene oxide, Electrochimica Acta. 125 (2014) 38-47. https://doi.org/10.1016/j.electacta.2014.01.074.

[12] M. Yola, N. Atar, Functionalized Graphene Quantum Dots with Bi-Metallic Nanoparticles Composite: Sensor Application for Simultaneous Determination of Ascorbic Acid, Dopamine, Uric Acid and Tryptophan, Journal Of The Electrochemical Society. 163 (2016) B718-B725. https://doi.org/10.1149/2.1191614jes.

[13] S. Elçin, M. Yola, T. Eren, B. Girgin, N. Atar, Highly Selective and Sensitive Voltammetric Sensor Based on Ruthenium Nanoparticle Anchored Calix[4]amidocrown-5 Functionalized Reduced Graphene Oxide: Simultaneous Determination of Quercetin, Morin and Rutin in Grape Wine, Electroanalysis. 28 (2015) 611-619. https://doi.org/10.1002/elan.201500495.

[14] K. Saha, S. Agasti, C. Kim, X. Li, V. Rotello, Gold Nanoparticles in Chemical and Biological Sensing, Chemical Reviews. 112 (2012) 2739-2779. https://doi.org/10.1021/cr2001178.

[15] M. OYAMA, Recent Nanoarchitectures in Metal Nanoparticle-modified Electrodes for Electroanalysis, Analytical Sciences. 26 (2010) 1-12. https://doi.org/10.2116/analsci.26.1.

[16] M. Yola, N. Atar, A novel voltammetric sensor based on gold nanoparticles involved in p-aminothiophenol functionalized multi-walled carbon nanotubes: Application to the simultaneous determination of quercetin and rutin, Electrochimica Acta. 119 (2014) 24-31. https://doi.org/10.1016/j.electacta.2013.12.028.

[17] H. Erikson, A. Sarapuu, K. Tammeveski, J. Solla-Gullón, J. Feliu, Shape-Dependent Electrocatalysis: Oxygen Reduction on Carbon-Supported Gold Nanoparticles, Chemelectrochem. 1 (2014) 1338-1347. https://doi.org/10.1002/celc.201402013.

[18] G. Gotti, K. Fajerwerg, D. Evrard, P. Gros, Electrodeposited gold nanoparticles on glassy carbon: Correlation between nanoparticles characteristics and oxygen reduction kinetics in neutral media, Electrochimica Acta. 128 (2014) 412-419. https://doi.org/10.1016/j.electacta.2013.10.172.

[19] D. Geng, G. Lu, Size effect of gold nanoparticles on the electrocatalytic oxidation of carbon monoxide in alkaline solution, Journal Of Nanoparticle Research. 9 (2007) 1145-1151. https://doi.org/10.1007/s11051-007-9210-1.

[20] H. Cheng, Application of Gold Nanoparticles and Nano-Diamond Modified Electrode for Hemoglobin Electrochemistry, International Journal Of Electrochemical Science. 15 (2020) 11416-11426. https://doi.org/10.20964/2020.11.15.

[21] KINOSHITA, K. *Electrochemical Oxygen Technology*. John Wiley & Sons, Inc.: New York, 1992, 462. ISBN:978-0-471-57043-1.

[22] U. Paulus, A. Wokaun, G. Scherer, T. Schmidt, V. Stamenkovic, V. Radmilovic et al., Oxygen Reduction on Carbon-Supported Pt−Ni and Pt−Co Alloy Catalysts, The Journal Of Physical Chemistry B. 106 (2002) 4181-4191. https://doi.org/10.1021/jp013442l.

[23] ADZIC, R. *Recent advances in the kinetics of oxygen reduction*. in: J. Lipkowski, P.N. Ross (Eds.), Electrocatalysis, Wiley-VCH, New York, 1998,197–242.

[24] [24] M. Shao, Electrocatalysis in Fuel Cells, Catalysts. 5 (2015) 2115-2121. https://doi.org/10.3390/catal5042115.

[25] R.R. Adžić, N.M. Marković, V.B. Vešović, Structural effect in electrocatalysis: oxygen reduction on the Au(100) single crystal electrode, J. Electroanal. Chem. 165 (1984) 105–120. http://dx.doi.org/10.1016/S0022-0728%2884%2980090-X.

[26] M. Valden, X. Lai, D.W. Goodman, Onset of Catalytic Activity of Gold Clusters on Titania with the Appearance of Nonmetallic Properties, Science 281 (1998) 1647-1650. http://dx.doi.org/10.1126/science.281.5383.1647.

[27] N. Lopez, T.V.W. Janssens, B.S. Clausen, Y. Xu, M. Mavrikakis, T. Bligaard, J.K. Nørskov, On the origin of the catalytic activity of gold nanoparticles for low-temperature CO oxidation, J. Catal. 223 (2004) 232–235. http://dx.doi.org/10.1016/j.jcat.2004.01.001.

[28] TRASATTI, S. *Interfacial Electrochemistry of Conductive Oxides for Electrocatalysis*, in: A. Wieckowski (Ed.), Interfacial Electrochemistry, Theory, Experiment and Applications, Marcel Dekker Inc., New York, 1999, 769−793.

[29] M. Haruta, S. Tsubota, T. Kobayashi, H. Kageyama, M.J. Genet, B. Delmon, Low-Temperature Oxidation of CO over Gold Supported on TiO_2, α-Fe_2O_3 and Co_3O_4, J. Catal. 144 (1993) 175–192. http://dx.doi.org/10.1006/jcat.1993.1322.

[30] S. Tsubota, D.A.H. Cunningham, Y. Bando, M. Haruta, Preparation of nanometer gold strongly interacted with TiO_2 and the structure sensitivity in low-temperature oxidation of CO, Stud. Surf. Sci. Catal. 91 (1995) 227–235. http://dx.doi.org/10.1016/S0167-2991%2806%2981759-3.

[31] F. Conte , I. Rossetti, G. Ramis , C. Vaulot , S. Hajjar-Garreau and S Bennici, Low Metal Loading (Au, Ag, Pt, Pd) Photo-Catalysts Supported on TiO_2 for Renewable Processes, Materials. 15 (2022) 2915. https://doi.org/10.3390/ma15082915.

[32] S.G. Neophytides, S.H. Zafeiratos, M.M. Jaksic, Selective Interactive Grafting of Composite Bifunctional Electrocatalysts for Simultaneous Anodic Hydrogen and CO Oxidation: I. Concepts and Embodiment of Novel-Type Composite Catalyst, J. Electrochem. Soc. 150 (2003) E512−E526. http://dx.doi.org/10.1149/1.1606456.

[33] J.M. Macak, F. Schmidt-Stein, P. Schmuki, Efficient oxygen reduction on layers of ordered TiO_2 nanotubes loaded with Au nanoparticles, Electrochem. Commun. 9 (2007) 1783–1787. http://dx.doi.org/10.1016/j.elecom.2007.04.002.

[34] M. Momeni, Y. Ghayeb, Fabrication, characterization and photocatalytic properties of Au/TiO_2-WO_3 nanotubular composite synthesized by photo-assisted deposition and electrochemical anodizing methods, Journal Of Molecular Catalysis A: Chemical. 417 (2016) 107-115. http://dx.doi.org/10.1016/j.molcata.2016.03.024.

[35] M. Momeni, Fabrication of copper decorated tungsten oxide–titanium oxide nanotubes by photochemical deposition technique and their photocatalytic application under visible light, Applied Surface Science. 357 (2015) 160-166. http://dx.doi.org/10.1016/j.apsusc.2015.09.015.

[36] M. Momeni, Y. Ghayeb, Cobalt modified tungsten–titania nanotube composite photoanodes for photoelectrochemical solar water splitting, Journal Of Materials Science: Materials In Electronics. 27 (2015) 3318-3327. http://dx.doi.org/10.1007/s10854-015-4161-2.

[37] S. Angkaew, P. Limsuwan, Preparation of silver-titanium dioxide core-shell (Ag@TiO_2) nanoparticles: Effect of Ti-Ag mole ratio, Procedia Engineering. 32 (2012) 649-655. http://dx.doi.org/10.1016/j.proeng.2012.01.1322.

[38] P. Martins, S. Kappert, H. Nga Le, V. Sebastian, K. Kühn, M. Alves et al., Enhanced Photocatalytic Activity of Au/TiO_2 Nanoparticles against Ciprofloxacin, Catalysts. 10 (2020) 234. http://dx.doi.org/10.3390/catal10020234.

[39] Z. Bian, T. Tachikawa, W. Kim, W. Choi, T. Majima, Superior Electron Transport and Photocatalytic Abilities of Metal-Nanoparticle-Loaded TiO_2 Superstructures, The Journal Of Physical Chemistry C. 116 (2012) 25444-25453. http://dx.doi.org/10.1021/jp309683f.

[40] K. Rajeshwar, M.E. Osugi, W. Chanmanee, C.R. Chenthamarakshan, M.V.B. Zanoni, P. Kajitvichyanukul, R. Krishnan-Ayer, Heterogeneous photocatalytic treatment of organic dyes in air and aqueous media, Journal of Photochemistry and Photobiology C: Photochemistry Reviews. 9 (2008) 171–192. https://doi.org/10.1016/j.jphotochemrev.2008.09.001

[41] M.D. Hernández-Alonso, F. Fresno, S. Suárez, J.M. Coronado, Development of alternative photocatalysts to TiO_2: Challenges and opportunities, Energy & Environmental Science. 2 (2009) 1231–1257. https://doi.org/10.1039/b907933e.

[42] H. Chen, L. Wang, Nanostructure sensitization of transition metal oxides for visible-light photocatalysis, Beilstein Journal of Nanotechnology. 5 (2014) 696–710. https://doi.org/10.3762/bjnano.5.82.

[43] D.B. Ingram, S. Linic, Water Splitting on Composite Plasmonic Metal/Semiconductor Photoelectrodes: Evidence for Selective Plasmon-Induced Formation of Charge Carriers near the Semiconductor Surface, Journal of the American Chemical Society. 133 (2011) 5202–5205. https://doi.org/10.1021/ja200086g.

[44] L. Jiang, G. Zhou, J. Mi, Z. Wu, Fabrication of visible-light-driven one- dimensional anatase TiO_2/Ag heterojunction plasmonic photocatalyst, Catalysis Communications. 24 (2012) 48-51. https://doi.org/10.1016/j.catcom.2012.03.017.

[45] R. Tripathi, A. Shrivastav, B. Shrivastav, Biogenic gold nanoparticles: As a potential candidate for brain tumor directed drug delivery, Artificial Cells, Nanomedicine, And Biotechnology. 43 (2014) 311-317. https://doi.org/10.3109/21691401.2014.885445.

[46] S. Donga, G. Bhadu, S. Chanda, Antimicrobial, antioxidant and anticancer activities of gold nanoparticles green synthesized using Mangifera indica seed aqueous extract, Artificial Cells, Nanomedicine And Biotechnology. 48 (2020) 1315-1325. https://doi.org/10.1080/21691401.2020.1843470.

[47] F. Milanezi, L. Meireles, M. de Christo Scherer, J. de Oliveira, A. da Silva, M. de Araujo et al., Antioxidant, antimicrobial and cytotoxic activities of gold nanoparticles capped with quercetin, Saudi Pharmaceutical Journal. 27 (2019) 968-974. https://doi.org/10.1016/j.jsps.2019.07.005.

[48] R. Vijayan, S. Joseph, B. Mathew, Anticancer, antimicrobial, antioxidant, and catalytic activities of green-synthesized silver and gold nanoparticles using Bauhinia purpurea leaf extract, Bioprocess And Biosystems Engineering. 42 (2018) 305-319. https://doi.org/10.1007/s00449-018-2035-8.

[49] A. Chahardoli, N. Karimi, F. Sadeghi, A. Fattahi, Green approach for synthesis of gold nanoparticles from Nigella arvensis leaf extract and evaluation of their antibacterial, antioxidant, cytotoxicity and catalytic activities, Artificial Cells, Nanomedicine, And Biotechnology. 46 (2017) 579-588. https://doi.org/10.1080/21691401.2017.1332634.

[50] E. Ahn, S. Hwang, M. Choi, S. Cho, H. Lee, Y. Park, Upcycling of jellyfish (Nemopilema nomurai) sea wastes as highly valuable reducing agents for green synthesis of gold nanoparticles and their antitumor and anti-inflammatory activity, Artificial Cells, Nanomedicine, And Biotechnology. 46 (2018) 1127-1136. https://doi.org/10.1080/21691401.2018.1480490.

[51] Yasmin M.S. Jamil, Mohammed Ahmed Hussein Awad, Hussein M.A. Al-Maydama, Ahmed N. Alhakimi , Mohamad M.E. Shakdofa, Samir Osman Mohammed, Gold nanoparticles loaded on TiO_2 nanoparticles doped with N_2 as an efficient electrocatalyst for glucose oxidation: preparation, characterization, and electrocatalytic properties, Journal of Analytical Science and Technology 13(54) (2022). https://doi.org/10.1186/s40543-022-00363-0.

[52] V. González, B. Kharisov, I. Gómez, Preparation, optical characterization and stability of gold nanoparticles by facile methods, Revista Mexicana De Física. 65 (2019) 690-698. https://doi.org/10.31349/RevMexFis.65.690.

[53] V. Pifferi, A. Testolin, C. Ingrosso, M. Lucia. Curri, I. Palchetti and L. Falciola, Au Nanoparticles Decorated Graphene-Based Hybrid Nanocomposite for As(III) Electroanalytical

Detection. Chemosensors. 10 (2022) 67. https://doi.org/10.3390/chemosensors10020067.

[54] W. Wang, J. Chen, Z. Zhou, S. Zhan, Z. Xing, H. Liu and L. Zhang, Ultrasensitive and Selective Detection of Glutathione by Ammonium Carbamate–Gold Platinum Nanoparticles-Based Electrochemical Sensor. Life. 12(2022) 1142. https://doi.org/10.3390/life12081142.

[55] A.J. Bard, L.R. Faulkner, Elecrochemical Methods Fundamentals and Applications, 2nd ed., Wiley, New York, 2004. ISBN:8126508078, 9788126508075.

[56] Mir. Ghasem. Hosseini, Mohamad. Mohsen. Momeni and Solmaz. Zeynali, Au Nanoparticle-Doped TiO_2 Nanotubes Catalysts Prepared by Anodizing and Electroplating Methods and Its Application for Nitrite Detection. Journal of Materials Science and Engineering B 2 (1) (2012) 16-23.

[57] I. Georgiana. Munteanu and C. Apetrei, Tyrosinase-Based Biosensor—A New Tool for Chlorogenic Acid Detection in Nutraceutical Formulations. Materials. 15 (2022) 3221. https://doi.org/10.3390/ma15093221.

[58] B. BEDEN, Electrocatalytic oxidation of saturated oxygenated compounds on gold electrodes*1, Journal Of Catalysis. 104 (1987) 37-46. https://doi.org/10.1016/0021-9517(87)90334-4.

[59] B. Wang, L. Tao, Y. Cheng, F. Yang, Y. Jin, C. Zhou et al., Electrocatalytic Oxidation of Small Molecule Alcohols over Pt, Pd, and Au Catalysts: The Effect of Alcohol's Hydrogen Bond Donation Ability and Molecular Structure Properties, Catalysts. 9 (2019) 387. https://doi.org/10.3390/catal9040387.

[60] M. Hsiao, R. Adžić, E. Yeager, Electrochemical Oxidation of Glucose on Single Crystal and Polycrystalline Gold Surfaces in Phosphate Buffer, Journal Of The Electrochemical Society. 143 (1996) 759-767. https://doi.org/10.1149/1.1836536.

[61] C. Xiang, Q. Xie, S. Yao, Electrochemical Quartz Crystal Impedance Study of Glucose Oxidation on a Nickel Hydroxide Modified Au Electrode in Alkaline Solution, Electroanalysis. 15 (2003) 987-990. https://doi.org/10.1002/elan.200390120.

[62] L. Burke, J. Moran, P. Nugent, Cyclic voltammetry responses of metastable gold electrodes in aqueous media, Journal Of Solid State Electrochemistry. 7 (2003) 529-538. https://doi.org/10.1007/s10008-003-0359-y.

[63] Y. M. S. Jamil, M. A. H. Awad, H. M. A. Al-Maydama, Y. EL-Ghoul, A. N. Al-Hakimi, Synthesis and study of enhanced electrochemical properties of NiO nanoparticles deposited on TiO_2 nanotubes, Applied Organometallic Chemistry. 36 (9) (2022) e6795,1-15. https://doi.org/10.1002/aoc.6795.

[64] U. Schmidt, M. Donten, J. Osteryoung, Gold Electrocrystallization on Carbon and Highly Oriented Pyrolytic Graphite from Concentrated Solutions of LiCl, Journal Of The Electrochemical Society. 144 (1997) 2013-2021 https://doi.org/10.1149/1.1837736.

[65] M. Finot, G. Braybrook, M. McDermott, Characterization of electrochemically deposited gold nanocrystals on glassy carbon electrodes, Journal Of Electroanalytical Chemistry. 466 (1999) 234-241. https://doi.org/10.1016/s0022-0728(99)00154-0.

[66] M. El-Deab, T. Ohsaka, Hydrodynamic voltammetric studies of the oxygen reduction at gold nanoparticles-electrodeposited gold electrodes, Electrochimica Acta. 47 (2002) 4255-4261. https://doi.org/10.1016/s0013-4686(02)00487-5.

[67] A. Liu, J. Zhu, J. Han, H. Wu, C. Jiang, Fabrication and characterization of gold nanoclusters on phosphorus incorporated tetrahedral amorphous carbon electrode, Electrochemistry Communications. 10 (2008) 827-830. https://doi.org/10.1016/j.elecom.2008.03.012.

[68] M. Nicol, The anodic behaviour of gold, Gold Bulletin. 13 (1980) 46-55. https://doi.org/10.1007/bf03215452.

[69] A.M. Siti Norsafurah, M. Yusairie, J. Khairil Anuar , Synthesis and Electrocatalytic Activity of Pt/Ni/Ti Electrocatalyst for Methanol Oxidation in alkaline Medium. Australian Journal of Basic and Applied Sciences. 9 (29) (2015) 9-15. http://www.ajbasweb.com/.